

# A New Analytical Diode Model Including Tunneling and Avalanche Breakdown

G. A. M. Hurkx, H. C. de Graaff, W. J. Kloosterman, and M. P. G. Knuyvers

**Abstract**—A new analytical model describing reverse and forward dc diode characteristics is presented. It serves as a basis for a compact model for circuit simulation purposes. The model is based on the solution of the hole continuity equation in the depletion layer of a p-n junction and incorporates the following physical mechanisms: band-to-band tunneling, trap-assisted tunneling (both under forward and reverse bias), Shockley-Read-Hall recombination, and avalanche breakdown. It contains seven parameters which can be determined at one temperature. No additional parameters are needed to describe the temperature dependence. From comparisons with both numerical simulations and measurements it is found that the model gives an adequate description of the dc characteristics in both forward and reverse modes.

## I. INTRODUCTION

AT HIGH dopant concentrations tunneling effects can influence the reverse and low tunneling diode  $I$ - $V$  characteristics. Not only band-to-band tunneling but also tunneling via traps can be important [1]–[4]. Fig. 1 shows measured reverse and forward  $I$ - $V$  characteristics of three different diodes with a breakdown voltage in the range of 5–15 V. From this figure it is apparent that while the forward characteristics are fairly similar, the reverse characteristics are quite different. Not only do the values of the current at a certain voltage differ by several orders of magnitude, but the shapes of the characteristics are also different. Moreover, the temperature dependencies of these characteristics are also quite different (see Fig. 6).

Existing compact models such as that in SPICE or extensions of it [5] usually give a nearly constant reverse current up to a certain breakdown voltage. Beyond breakdown the characteristic is described by one (SPICE) or more exponential functions. When tunneling is important (i.e., for diodes with a low breakdown voltage), such a description is fairly poor. Moreover, also the modeling of the temperature dependence is poor because of the assumed dependence of the reverse current on the ideal saturation current. In this paper we present a new dc model for circuit simulation purposes which incorporates the following physical mechanisms: band-to-band tunneling, trap-assisted tunneling, Shockley-Read-Hall recombination, and avalanche breakdown.

Manuscript received November 6, 1991; revised February 10, 1992. The review of this paper was arranged by Associate Editor D. D. Tang. The authors are with Philips Research Laboratories, 5600 JA Eindhoven, The Netherlands.  
IEEE Log Number 9201804.

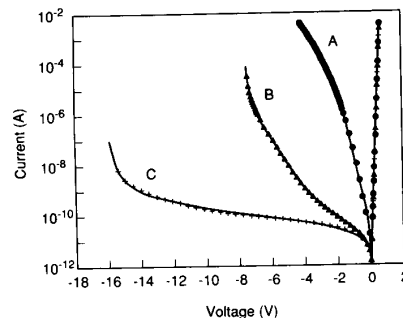


Fig. 1. Forward and reverse  $I$ - $V$  characteristics of three different diodes. The absolute value of the current is plotted. Both measurements (symbols) and model calculations (solid lines) are denoted.

The model is based on the solution of the hole continuity equation in the depletion layer of a p-n junction. The boundary conditions as well as the expressions for the different recombination mechanisms are described in Section II. In Section III the model expressions for reverse and forward bias are derived. In Section IV a comparison is made between one-dimensional (1D) numerical device simulations and model calculations. The model parameters and their temperature dependence are discussed in Section V. In Section VI model results are presented.

## II. MODEL BASIS

The 1D steady-state continuity equation for holes in the depletion layer of a p-n junction reads

$$\frac{dJ_p}{dx} = -qR_{\text{tot}}(x) \quad (1)$$

where  $J_p(x)$  is the hole current density and  $R_{\text{tot}}(x)$  is the total net recombination rate. Obviously, the choice of the continuity equation for holes as a starting point is arbitrary. We can also start with the continuity equation for electrons, leading to equivalent results. The boundary conditions are (see Fig. 2)

$$J_p(-x_p) = J_d - J_{np} \quad (2a)$$

$$J_p(x_n) = J_{pn} \quad (2b)$$

where  $J_{np}$  and  $J_{pn}$  are the ideal electron and hole current densities due to recombination in the neutral p and n regions, respectively. The boundaries of the depletion layer at the p side and at the n side are denoted by  $-x_p$  and  $x_n$ ,

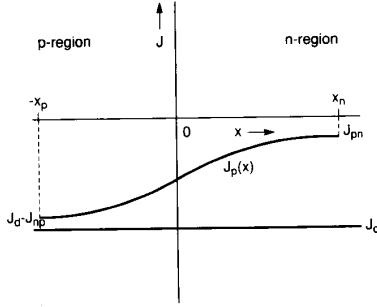


Fig. 2. Distribution of the hole current density in the depletion layer around a p-n junction under reverse bias conditions. The metallurgical junction is at  $x = 0$ .

respectively. The total diode current density  $J_d$  is, of course, independent of the position  $x$ .

The total net recombination rate consists of the following contributions:

- Avalanche multiplication  $R_{av}(x)$ . For this term we use

$$R_{av}(x) = \frac{-1}{q} \{ \alpha_n(x) |J_n(x)| + \alpha_p(x) |J_p(x)| \}. \quad (3)$$

The quantities  $\alpha_n(x)$  and  $\alpha_p(x)$  are the ionization coefficients for electrons and holes, respectively. We will return to the expression for their field dependence in Section III-A.

- Band-to-band tunnelling  $R_{bbt}(x)$ . This mechanism describes transitions of electrons which tunnel directly from the valence band to the conduction band [6], [7]. This mechanism dominates the reverse characteristics of heavily doped diodes with a breakdown voltage below approximately 6 V. For very heavily doped diodes (Esaki diodes) this mechanism is also apparent in the low forward bias regime.

- Recombination via traps  $R_{trap}(x)$ . This term, which contains not only the conventional Shockley-Read-Hall mechanism but also tunneling via traps [1]–[4], is given by

$$R_{trap}(x) = (1 + \Gamma(x)) R_{SRH}(x). \quad (4)$$

The function  $\Gamma$ , which accounts for the effects of tunneling on both the density of captured carriers by a trap and the emission rate of carriers from a trap, is given by

$$\Gamma = 2\sqrt{3}\pi \frac{|F|}{F_\Gamma} \exp(F/F_\Gamma)^2 \quad (5)$$

with

$$F_\Gamma = \frac{\sqrt{24m^*(kT)^3}}{q\hbar} \quad (6)$$

where  $F$  is the local electric field and  $m^*$  ( $m^* = 0.25m_0$  [8]) is the effective mass of the carriers. A derivation of (5) is given in [8]. This expression is valid for  $F < F_\Gamma (\Delta E/3kT)^{1/2}$ , where  $\Delta E$  is related to the trap level and under reverse bias conditions equal to  $E_g/2$  for midgap states [8]. For stronger electric fields (i.e., stronger than

approximately  $9 \times 10^5$  V/cm at room temperature), (5) overestimates the actual value of  $\Gamma$ . However, at such a strong electric field band-to-band tunneling dominates and recombination via traps is unimportant. Under forward bias the second term on the right-hand side of (4) describes the so-called forward-bias tunneling current or excess current. The term  $R_{SRH}(x)$  is the conventional SRH recombination rate given by

$$R_{SRH}(x) = \frac{pn - n_{ie}^2}{\tau_p(n + n_1) + \tau_n(p + p_1)} \quad (7)$$

with  $p$  and  $n$  the hole and electron densities, respectively. The quantities  $\tau_p$  and  $\tau_n$  are the lifetimes, while  $p_1$  and  $n_1$  are given by  $p_1 = n_{ie} \exp[(E_T - E_i)/kT]$  and  $n_1 = n_{ie} \exp[-(E_T - E_i)/kT]$ , where  $n_{ie}$  is the intrinsic carrier concentration,  $E_T$  is the trap level, and  $E_i$  is the intrinsic Fermi level. For weak electric fields, i.e.,  $F \ll 10^5$  V/cm at room temperature,  $\Gamma \ll 1$  and (4) reduces to the conventional SRH recombination rate.

### III. MODEL DERIVATION

#### A. Reverse Bias

The substitution of (3) for avalanche multiplication into (1) yields a first-order inhomogeneous differential equation. Using  $J_d = J_n(x) + J_p(x)$  and boundary condition (2a), this equation can be solved exactly (e.g., see [9], [10]) to give an expression for  $J_p(x)$ . By using boundary condition (2b) the diode current density can be found. This yields

$$J_d = \frac{J_{np} + J_{pn}\phi(x_n) + q \int_{-x_p}^{x_n} (R_{trap}(x) + R_{bbt}(x))\phi(x) dx}{1 - \int_{-x_p}^{x_n} \alpha_n(x)\phi(x) dx}, \quad (8)$$

with

$$\phi(x) = \exp \left[ - \int_{-x_p}^x (\alpha_n - \alpha_p) dx' \right]. \quad (9)$$

To arrive at a compact model expression which is suitable for circuit simulation purposes the following steps are taken:

- 1) The band-to-band tunneling term is taken into account as a Dirac  $\delta$ -function generation term at the location of the maximum electric field, i.e.,

$$R_{bbt}(x) = \frac{J_{bbt}}{q} \delta(x) \quad (10)$$

where the band-to-band tunneling current density  $J_{bbt}$  is given by [11]

$$J_{bbt} = c_{bbt} V_j (F_m/F_0)^{3/2} e^{-F_0/F_m} \quad (11)$$

with  $F_m$  the maximum electric field (i.e., the field at  $x = 0$ ) and  $F_0$  a constant which depends on the temperature through the temperature dependence of the bandgap ( $F_0$

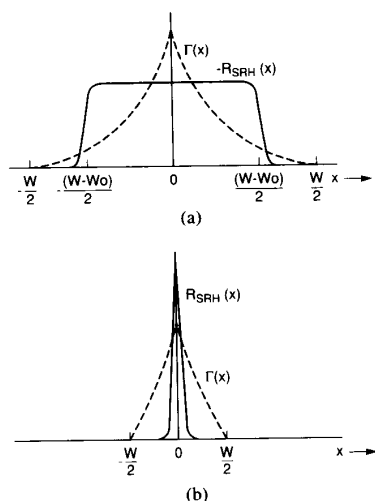


Fig. 3. Behavior of the field-effect function  $\Gamma(x)$  (see (5)) and the recombination rate  $R_{SRH}(x)$  in the depletion layer of a symmetrical p-n junction under reverse (a) and forward (b) bias.

$\sim E_g^{3/2}$ ) and which has at room temperature a value of  $1.9 \times 10^7$  V/cm. The prefactor  $c_{bbt}$  is taken to be temperature-independent. Under reverse bias the junction voltage  $V_j$  is taken to be negative.

2) Due to the strong dependence of  $\Gamma$  on the local electric field, the second term on the right-hand side of (4) has a sharp maximum at  $x = 0$  (see Fig. 3(a)). For this reason also this term, which accounts for tunneling via traps, is accounted for as a  $\delta$ -function generation term  $J_{iat} \delta(x)$  at the location of the maximum electric field, with  $J_{iat}$  given by

$$J_{iat} = q \int_{-x_p}^{x_n} R_{SRH}(x) \Gamma(x) dx. \quad (12)$$

Now (8) becomes

$$J_d = \frac{J_{np} + J_{pn} \phi(x_n) + (J_{bbt} + J_{iat}) \phi(0) + q \int_{-x_p}^{x_n} R_{SRH}(x) \phi(x) dx}{1 - \int_{-x_p}^{x_n} \alpha_n(x) \phi(x) dx}. \quad (13)$$

Up to now we have no assumption concerning the type of junction. However, to obtain practical expressions for  $J_{iat}$  and the integrals in (13), we assume a symmetrical step junction. This assumption does not limit the applicability of the model to other types of junctions, as can be seen from a comparison of model results with numerical simulations and measurements (Sections IV and VI). The electric field distribution is now given by

$$F(x) = F_m \left( 1 - \frac{2|x|}{W} \right) \quad (14)$$

where  $W$  is the depletion layer width.

3) The quantity  $R_{SRH}$  is under reverse bias approximately constant in the depletion region except within a

distance of  $W_0/2$  from the depletion-layer boundaries [12], where  $W_0$  is the zero-bias depletion layer width (see Fig. 3(a)). This behavior is approximated by (see (7))

$$R_{SRH} = \frac{-n_{ie}}{2\tau \cosh[(E_T - E_i)/kT]} \equiv -c_{SRH},$$

$$-(W - W_0)/2 < x < (W - W_0)/2 \quad (15)$$

and  $R_{SRH} = 0$  for  $x \leq -(W - W_0)/2$  and for  $x \geq (W - W_0)/2$ . The electron and hole lifetimes have been replaced by a single value  $\tau$ . Consequently

$$J_{SRH} = q \int_{-W/2}^{W/2} R_{SRH}(x) dx = -qc_{SRH}(W - W_0). \quad (16)$$

4) Using (15), (12) for  $J_{iat}$  becomes

$$J_{iat} = -qc_{SRH} \int_{-(W - W_0)/2}^{(W - W_0)/2} \Gamma(x) dx. \quad (17)$$

By the substitution of (14) for the electric field distribution into (5) for  $\Gamma(x)$ , subsequent substitution of the result into (17) and transformation to the integration variable  $F$ , we obtain after integration

$$J_{iat} = -q\sqrt{3\pi} c_{SRH} W \frac{F_\Gamma}{|F_m|} \cdot \left[ \exp\left(\frac{F_m}{F_\Gamma}\right)^2 - \exp\left(\frac{F_m W_0}{F_\Gamma W}\right)^2 \right]. \quad (18)$$

5) We write

$$J_{pn} = \beta J_i \quad (19a)$$

$$J_{np} = (1 - \beta) J_i \quad (19b)$$

where  $J_i$  is the ideal diode current density given by  $J_i = J_s (e^{qV_j/kT} - 1)$ ,  $J_s$  being the saturation current density. The value of  $\beta$  depends on the type of junction and varies

between 0 and 1. In forward bias the value of  $\beta$  is irrelevant, while in reverse bias the ideal current itself is not important for silicon diodes at room temperature. For these reasons the value of  $\beta$  is not critical and in the rest of this work  $\beta = 1/2$  is taken.

6) For the field dependence of the ionization coefficient the following well-known expression is used [13]:

$$\alpha_n = \alpha_{n\infty} \exp(-b_n/|F(x)|) \quad (20)$$

while we use a constant relation between  $\alpha_p$  and  $\alpha_n$ , i.e.,  $\alpha_p = \epsilon \alpha_n$ , with  $0 < \epsilon < 1$ . By the substitution of (14) for the electric field into (20) and subsequent substitution of the result into (9), the following approximation for  $\phi(x)$

can be found (see Appendix I):

$$\begin{aligned}\phi(x) &= 1, & x < 0 \\ &= \exp(-\mu_{av}), & x = 0 \\ &= \exp(-2\mu_{av}), & x > 0\end{aligned}\quad (21)$$

with  $\mu_{av}$  given by

$$\mu_{av} = (1 - \epsilon)d_{av}\alpha_{n\infty} \exp(-b_n/|F_m|) \quad (22)$$

where  $d_{av}$  is an effective length for avalanche multiplication (see (A4) of Appendix I).

When we substitute (16), (19), and (21) into (13), we arrive at the following model expression for the diode current density under reverse bias conditions:

$$J_d = \frac{(J_{bbr} + J_{iat})e^{-\mu_{av}} + (J_{SRH} + J_i)(1 + e^{-2\mu_{av}})/2}{1 - \frac{\mu_{av}}{1 - \epsilon}(1 + e^{-2\mu_{av}})} \quad (23)$$

The choice of the value of  $\epsilon$  has no strong influence on the model behavior. In the rest of this work we take  $\epsilon = 1/2$ . Breakdown occurs when the denominator of (23) becomes zero. This gives for  $\mu_{av}$  at breakdown a value of 0.3295. Normalizing (22) for  $\mu_{av}$  to this value at breakdown yields

$$\mu_{av} = 0.3295 \left(\frac{F_m}{F_{mbr}}\right)^2 \exp\left(b_n \frac{F_m - F_{mbr}}{F_m F_{mbr}}\right) \quad (24)$$

where  $F_{mbr}$  is the maximum field at breakdown. This expression has the advantages that the unknown quantity  $d_{av}$  is eliminated and that  $J_d$  becomes infinite at exactly the breakdown voltage. Equation (23) together with (11), (16), (18), and (24) form the basis of the model under reverse-bias conditions.

### B. Forward Bias

In forward bias only  $R_{trap}$  is taken into account. Integration of the continuity equation (1) and using boundary conditions (2a) and (2b) now yields

$$J_d = J_{np} + J_{pn} + q \int_{-x_p}^{x_n} R_{trap}(x) dx \quad (25)$$

which is the familiar sum of the ideal and nonideal contributions. To evaluate this term further we realize that contrary to the situation in reverse bias, in forward bias the function  $R_{SRH}(x)$  is much more sharply peaked than  $\Gamma(x)$  (see Fig. 3(b)). For this reason we can write

$$\int_{-x_p}^{x_n} R_{trap}(x) dx \approx (1 + \Gamma(d)) \int_{-x_p}^{x_n} R_{SRH}(x) dx \quad (26)$$

under forward bias, so the problem is reduced to the calculation of the conventional nonideal current. At the location  $x = d$  the electron and hole concentrations are equal. The value of  $d$  is close to zero and is for symmetrical junctions equal to zero, i.e., the location of the maximum field coincides with the location where  $p = n$ .

Different approximations for the integral in (26) (i.e., the nonideal current) are presented in the literature (e.g., [9], [14]). We use the expression derived in Appendix II, which provides also a good description under very low forward bias. This gives for the diode current density under forward bias

$$J_d = J_i + 2c_{SRH}(1 + \Gamma(d)) \frac{kT}{F(d)} \cosh\left(\frac{E_T - E_i}{kT}\right) \cdot \sinh\left(\frac{qV_j}{2kT}\right) \zeta(V_j) \quad (27)$$

where

$$\zeta(V_j) = \frac{2\pi}{t + 2} \quad (28)$$

with

$$t = \cosh\left(\frac{E_T - E_i}{kT}\right) \exp\left(\frac{-qV_j}{2kT}\right). \quad (29)$$

Under very low forward bias conditions the second term on the right-hand side of (27) shows nearly ideal behavior (see Appendix II), while otherwise it has the usual nonideal behavior and is for  $E_T = E_i$  equal to the expression given in [9]. The term with  $\Gamma(d)$  accounts for the forward-bias tunneling term which becomes important at room temperature for junctions with a zero-bias depletion-layer width below approximately 30 nm [8]. Equation (27) together with (28) and (29) form the basis of the model under forward-bias conditions.

## IV. COMPARISON OF ANALYTICAL CALCULATIONS WITH NUMERICAL SIMULATIONS

To test the validity of the mathematical simplifications involved, Fig. 4 shows a comparison of results from a 1D numerical device simulation with model results at 300 K. The corresponding doping profile is given in Fig. 5. In the device simulation program the recombination model for tunneling as described in [8] is used, together with the model for avalanche multiplication as given by (3). To obtain the analytical results, the numerically calculated values of  $F_m$  and  $W$  (from the depletion capacitance) at each bias point are used. Also the quantities  $F_{mbr}$ ,  $V_{br}$ ,  $J_s$ , and  $c_{SRH}$  are taken from the numerical simulations. For  $c_{SRH}$  the value of  $n_{ie}/\tau$  at the location where  $n = p$  is taken. The doping profile is chosen such that the breakdown voltage is around 8 V. In that case both recombination via traps and band-to-band tunneling are apparent in the reverse characteristics. This is shown in Fig. 4. From this figure we can observe that the agreement between numerical and analytical results is fairly good.

## V. PARAMETER DETERMINATION

For practical use the problem arises that due to dopant inhomogeneities the electric field generally will not be ex-

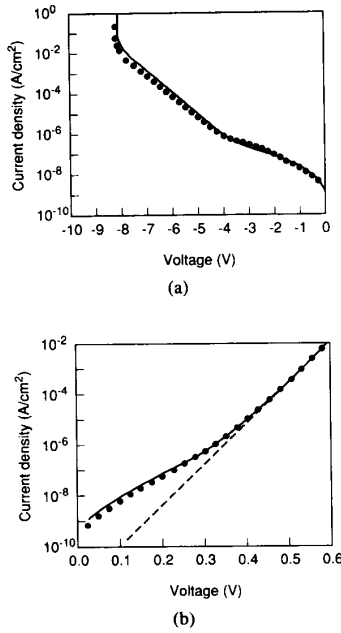


Fig. 4. A comparison of model results with numerical simulations of a diode number reverse (a) and forward (b) bias at  $T = 300$  K. The doping profile is given in Fig. 5. The dashed line denotes the ideal current  $J_i$ .

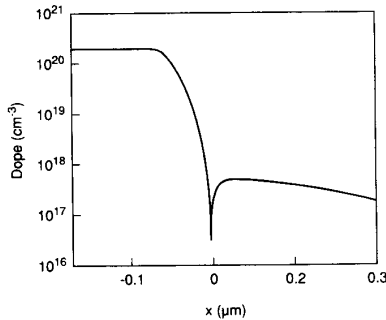


Fig. 5. The doping profile of the diode as used in the numerical simulations of Fig. 4.

actly constant along the junction area. Because tunneling effects and avalanche multiplication are extremely sensitive functions of the electric field, the current due to these effects is strongly confined to the area where the electric field is highest. This implies that the effective junction area is usually not equal to the macroscopic junction area. For this reason the following parameter determination strategy is followed for accurate modeling: The voltage dependence of the depletion capacitance is given by the quantities  $V_{int}$  and  $p$  which are determined by fitting the capacitance to the relation

$$C_d(V_j) = \frac{C_0}{(1 - V_j/V_{int})^p} \quad (30)$$

where  $C_0$  is the zero-bias capacitance. The depletion layer width is given by

$$W(V_j) = W_0(1 - V_j/V_{int})^p. \quad (31)$$

By the application of Gauss' law the maximum electric field as a function of the junction voltage is obtained by integrating the depletion capacitance [15]. This yields

$$\begin{aligned} F_m(V_j) &= \frac{V_{int}}{(1-p)W_0} (1 - V_j/V_{int})^{(1-p)} \\ &\equiv F_{m0}(1 - V_j/V_{int})^{(1-p)} \end{aligned} \quad (32)$$

where  $F_{m0}$  is the maximum electric field at zero bias. As can be seen from (31) and (32) the voltage dependencies of the depletion-layer width and the maximum electric field are determined by the parameters  $V_{int}$  and  $p$ , which are obtained from  $C$ - $V$  measurements. The magnitudes of these quantities are given by  $W_0$  and  $F_{m0}$ , which are related according to (32). Hence, only one of these quantities must be treated as a parameter. However, we have chosen the maximum electric field at breakdown  $F_{mbr}$  as the parameter to determine these quantities because it is easier to assess the physical significance of the resulting value for  $F_{mbr}$  (together with the value of the breakdown voltage) than that of  $W_0$  or  $F_{m0}$ . From (32) it follows that the relation between  $F_{m0}$  and  $F_{mbr}$  is given by

$$F_{m0} = F_{mbr}(1 - V_{br}/V_{int})^{(p-1)}. \quad (33)$$

The breakdown voltage  $V_{br}$  and the maximum field at breakdown  $F_{mbr}$ , together with the prefactors  $c_{bbt}$ ,  $c_{SRH}$ , and  $J_s$ , are treated as parameters, and are determined by a single least squares fit of the whole  $I$ - $V$  characteristics, comprising both forward and reverse bias. Each of the parameters is most sensitive to one particular part of the characteristics. The value of  $V_{br}$  follows from characteristic near breakdown, while the value of  $F_{mbr}$  is given by the voltage dependence of the current under reverse and low forward bias. The values of the prefactors are given by the magnitude of the current in the different bias regimes. In the usual case where the current and not the current density is fitted the above prefactors also contain the effective junction area. So, the values of all parameters are determined from  $C$ - $V$  and  $I$ - $V$  measurements and no information concerning the doping profile or geometry is needed. When this information is available it can be used to assess the physical significance of the resulting parameter values. To this end the effective junction area can be determined by the division of the zero-bias capacitance  $C_0$  by the capacitance per unit area following from  $W_0$ .

The parameters are determined at one temperature. For the temperature dependence of  $c_{SRH}$  the usual temperature dependence of  $n_{ie}$  [16] is taken, while for the temperature dependence of  $J_s$  the temperature dependence of  $n_{ie}^2$  is used with a value of the bandgap  $E_g = 1$  eV and  $E_T = E_i$ . Furthermore,  $c_{bbt}$  is assumed to be temperature-independent while  $b_n$  and  $V_{br}$  have a weak temperature dependence according to values given in [17], [18].

## VI. RESULTS

Fig. 1 shows a comparison of model results with measurements on three  $p^{++}-n^{+}$  Zener diodes. These diodes have a large junction area ( $200 \times 200 \mu\text{m}^2$  for diode *A* and  $180 \times 180 \mu\text{m}^2$  for diodes *B* and *C*). Sidewall effects are eliminated by the use of a guard ring. The difference in breakdown voltage between these diodes is achieved by different  $n^{+}$  concentrations. Diode *A* has a constant  $n^{+}$  concentration of around  $10^{19} \text{cm}^{-3}$  while diodes *B* and *C* have a diffused  $n^{+}$  region with a lower top dope concentration. Furthermore, the specified reverse characteristic is for each type of diode obtained by a final diffusion step. These diodes have a nearly linearly graded junction. Fig. 6(a)–(c) shows the  $I$ - $V$  curves of these three diodes at three temperatures. From the temperature dependence of the currents we can observe that for diode *A* band-to-band tunneling dominates, while for diode *C* recombination via traps is important. For diode *B* we observe two distinct regions, as can be seen in Fig. 6. Notice the strong temperature dependence of the current at low bias due to the strong temperature dependence of  $n_{ie}$  and the weak temperature dependence at high bias conditions due to band-to-band tunneling and avalanche multiplication. The parameters are fitted for the curve at  $T = 338 \text{ K}$ , while the other curves are obtained without any fitting. The resulting parameter values are listed in Table I. Because the total current is fitted the prefactors  $c_{bbt}$ ,  $c_{SRH}$  and  $J_s$  contain the effective junction area. Fig. 6(a)–(c) shows that the temperature dependence of the currents is described fairly well by the model, without any additional fitting parameters for the temperature dependence. This means that in the parameter determination the model automatically selects the correct physical mechanism to describe the  $I$ - $V$  curve, i.e., for diode *A*— $c_{bbt}$ , for diode *C*— $c_{SRH}$ , while for diode *B* both terms are important. Fig. 7 shows results for diode *B* for the case where the trap-assisted tunneling term has been omitted in the model. The parameters are again determined at  $T = 338 \text{ K}$ . We see that in the low-bias regime the model is less accurate in that case. This is due to the fact that the voltage dependence of the SRH recombination term is too weak to describe the characteristic in this regime, while the voltage dependence of the band-to-band tunneling term is too strong. Thus in situations where the electric field is fairly strong (but not so strong that band-to-band tunneling dominates), the inclusion of the trap-assisted tunneling term improves the model accuracy.

It is important that the temperature at which the parameters are determined is chosen such that all relevant parameters for the temperature range of interest can accurately be determined at that temperature. For instance, at low temperatures band-to-band tunneling dominates the reverse characteristics of diodes *A* and *B*. This implies for these diodes the temperature at which the parameters are determined must be chosen high enough to determine  $c_{SRH}$  sufficiently accurately. On the other hand, if we were interested in the modeling of diode *C* far below room tem-

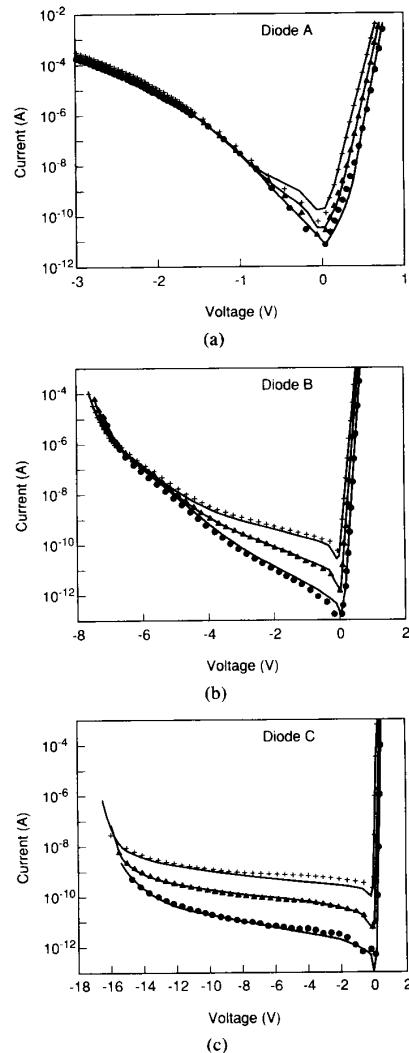


Fig. 6. Measured (symbols) and calculated (solid lines) characteristics of the diodes from Fig. 1 at three temperatures:  $\bullet$ :  $T = 294 \text{ K}$ ,  $\blacktriangle$ :  $T = 338 \text{ K}$ , and  $+$ :  $T = 383 \text{ K}$ . The parameters are determined from the  $I$ - $V$  characteristic at  $T = 338 \text{ K}$ .

TABLE I  
MODEL PARAMETERS AS OBTAINED BY FITTING THE MEASUREMENTS AT  
 $T = 338 \text{ K}$

Diode	A	B	C
$p$	0.336	0.314	0.283
$V_{ni}$ (V)	0.547	0.543	0.495
$F_{mbr}$ (MV/cm)	2.72	1.35	0.62
$V_{br}$ (V)	-4.75	-7.46	-15.88
$c_{bbt}$ (A/V)	8.33	3.96	—
$c_{SRH}$ ( $10^{12} \text{cm}^{-1} \cdot \text{s}^{-1}$ )	26.4	5.21	5.68
$J_s$ ( $10^{-13} \text{A}$ )	1.51	4.16	10.5

perature where band-to-band tunneling is significant, the choice of  $T = 338 \text{ K}$  would be obviously wrong and a corresponding temperature below room temperature should have been chosen.

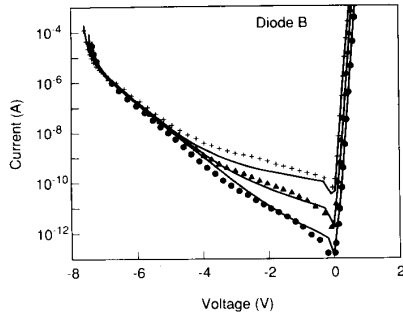


Fig. 7. Model results for diode *B* for the case where the trap-assisted tunneling term has been omitted in the model.

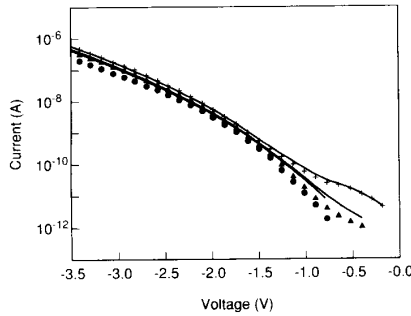


Fig. 8. Leakage currents of a reverse biased emitter-base junction of a bipolar transistor at three temperatures.  $\bullet$ :  $T = 294$  K,  $\blacktriangle$ :  $T = 329$  K, and  $+$ :  $T = 383$  K. The parameters are determined from the  $I$ - $V$  characteristic at  $T = 383$  K.

Under forward bias trap-assisted tunneling is only significant in diode *A*. This tunneling effect leads to a relatively large nonideal current which has a somewhat weaker temperature dependence than predicted by the conventional SRH mechanism. The nonideality factor is slightly larger than 2. This nonideal forward bias behavior is described in more detail in [8], where measurements on similar diodes are compared with numerical simulations.

The resulting values of the parameter  $c_{SRH}$  yield a value of  $\tau$  of a few microseconds for the three diodes. The resulting values of the maximum field at breakdown are  $2.72 \times 10^6$  V/cm,  $1.35 \times 10^6$  V/cm, and  $6.18 \times 10^5$  V/cm for diodes *A*, *B*, and *C*, respectively. These are realistic values for such highly doped diodes [16]. At the considered temperatures the ideal saturation current density  $J_s$  is found to be unimportant in reverse bias. The model accuracy can be slightly improved by allowing more model parameters. For instance, when  $E_g$  and  $E_T - E_i$  are also treated as parameters, the temperature dependence for diodes *B* and *C* improves. When the prefactor for the trap-assisted tunneling current  $J_{tat}$  is treated as a separate parameter, the description of the  $I$ - $V$  curves also slightly improves.

Finally, Fig. 8 shows the leakage currents at the emitter-base junction of a bipolar transistor at three temperatures. As expected, band-to-band tunneling dominates

these characteristics. The breakdown voltage could not be determined because of emitter-to-collector punchthrough.

## VII. SUMMARY

A new analytical model describing reverse and forward dc diode characteristics for circuit simulation purposes is presented. The model is based on the solution of the 1D steady-state continuity equation for holes in the depletion layer of a p-n junction. In the recombination rate band-to-band tunneling, trap-assisted tunneling, Shockley-Read-Hall recombination, and avalanche breakdown are incorporated. Although a number of approximations are involved, some of which are based on the assumption of a symmetrical step junction, the model results are in fairly good agreement with numerical simulations. Measurements on different types of p-n junctions showing distinctly different reverse bias behavior are described well by the model. It contains seven parameters which can be determined at one temperature. No additional parameters are needed to describe the temperature dependence.

## APPENDIX I

To write the ionization coefficient for electrons as a function of  $x$  we adopt the approach given in [19]. The substitution of (14) into (20) gives

$$\alpha_n(x) = \alpha_{n\infty} \exp \left[ \frac{-b_n}{|F_m| (1 - 2|x|/W)} \right] \quad (\text{A1})$$

which can be approximated by

$$\alpha_n(x) \approx \alpha_{n\infty} \exp \left[ \frac{-b_n}{|F_m|} (1 + 2|x|/W) \right] \quad (\text{A2})$$

for  $|x|/W \ll 1$ . This can be written as

$$\alpha_n(x) = \alpha_{n\infty} \exp(-b_n/|F_m| - |x|/d_{av}) \quad (\text{A3})$$

with

$$d_{av} = \frac{W|F_m|}{2b_n} = \frac{\epsilon_0 \epsilon_r F_m^2}{qNb_n} \quad (\text{A4})$$

where  $N$  is the dopant concentration of the symmetrical step junction. Substitution of (A3) into (9) for  $\phi(x)$  gives

$$\begin{aligned} \phi(x) &\approx \exp[-\mu_{av} \exp(x/d_{av})], & x < 0 \\ &\approx \exp[-\mu_{av}], & x = 0 \\ &\approx \exp[-\mu_{av}(2 - \exp(-x/d_{av}))], & x > 0 \end{aligned} \quad (\text{A5})$$

with  $\mu_{av}$  given by (22). Except for very strong electric fields it holds that  $d_{av} \ll W$  so that  $\alpha_n(x)$  and  $\phi(x)$  behave as sketched in Fig. 9. This behavior of  $\phi(x)$  can further be approximated by (21).

## APPENDIX II

To derive (27) we expand the potential  $\psi$  to first order around  $x = d$ , which is the location where  $p = n$ . The value of  $d$  is usually very small and is for symmetrical junctions equal to zero, i.e., the location of maximum

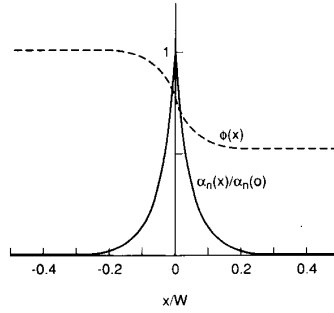


Fig. 9. A sketch of the functions  $\phi(x)$  and  $\alpha_n(x)/\alpha_n(0)$  in the depletion layer of a reverse biased junction.

field coincides with the location where  $p = n$ . This expansion gives

$$\psi(x) = \psi(d) - F(d)(x - d). \quad (A6)$$

At  $x = d$  it holds that

$$p(d) = n(d) = n_{ie} \exp(qV_j/2kT). \quad (A7)$$

From the Boltzmann relations it can now be derived that

$$n(x) = n_{ie} \exp\left(\frac{qV_j - 2qF(d)(x - d)}{2kT}\right) \quad (A8a)$$

$$p(x) = n_{ie} \exp\left(\frac{qV_j + 2qF(d)(x - d)}{2kT}\right) \quad (A8b)$$

where we have used the fact that under low forward bias the quasi-Fermi levels are constant across the depletion layer. After substitution of (A8) into (7), subsequent substitution of the result into (26), and replacing the integration boundaries by  $-\infty$  and  $\infty$ , we obtain after integration

$$q \int_{-x_p}^{x_n} R_{\text{trap}}(x) dx = 2c_{\text{SRH}}(1 + \Gamma(d)) \frac{kT}{F(d)} \cdot \cosh\left(\frac{E_T - E_i}{kT}\right) \sinh\left(\frac{qV_j}{2kT}\right) \zeta(V_j) \quad (A9)$$

with

$$\zeta(V_j) = \int_{-\infty}^{\infty} \frac{dy}{\cosh y + t}. \quad (A10)$$

Integration gives [20]

$$\begin{aligned} \zeta(V_j) &= \frac{2}{\sqrt{1-t^2}} \arccos t, & t < 1 \\ &= 2, & t = 1 \\ &= \frac{2}{\sqrt{t^2-1}} \arccos t, & t > 1. \end{aligned} \quad (A11)$$

The quantity  $t$  is given by (29). The above expression for  $\zeta(V_j)$  can be described sufficiently accurate by (28). For

$qV_j \gg 2(kT + |E_T - E_i|)$ ,  $t \ll 1$  and  $\zeta \rightarrow \pi$ , while for  $qV_j \ll 2(kT + |E_T - E_i|)$   $\zeta$  is roughly proportional to  $\exp(qV_j/2kT)$ .

#### REFERENCES

- [1] E. Hackbarth and D. D. Tang, "Inherent and stress-induced leakage in heavily doped silicon junctions," *IEEE Trans. Electron Devices*, vol. 35, no. 12, pp. 2108-2118, 1988.
- [2] J. A. Del Alamo and R. M. Swanson, "Forward-bias tunneling: A limitation to bipolar device scaling," *IEEE Electron Device Lett.*, vol. EDL-7, no. 11, pp. 629-631, 1986.
- [3] G. Vincent, A. Chantre, and D. Bois, "Electric field on the thermal emission of traps in semiconductor junctions," *J. Appl. Phys.*, vol. 50, no. 8, pp. 5484-5487, 1979.
- [4] G. A. M. Hurkx, D. B. M. Klaassen, M. P. G. Knuvers, and F. G. O'Hara, "A new recombination model describing heavy-doping effects and low-temperature behaviour," in *IEDM Tech. Dig.* (Washington, DC), 1989, pp. 307-310.
- [5] A. K. Laha and D. W. Smart, "A Zener diode model with application to SPICE2," *IEEE J. Solid-State Circuits*, vol. SC-16, no. 1, pp. 21-22, 1981.
- [6] E. O. Kane, "Theory of tunneling," *J. Appl. Phys.*, vol. 32, no. 1, pp. 83-89, 1961.
- [7] L. V. Keldysh, "Influence of the lattice vibrations of a crystal on the production of electron-hole pairs in strong electric fields," *Soviet Phys-JETP*, vol. 34, no. 4, pp. 665-668, 1958.
- [8] G. A. M. Hurkx, D. B. M. Klaassen, and M. P. G. Knuvers, "A new recombination model for device simulation including tunneling," *IEEE Trans. Electron Devices*, vol. 39, pp. 331-338, Feb. 1992.
- [9] C.-T. Sah, N. Noyce, and W. Shockley, "Carrier generation and recombination in p-n junctions and p-n junction characteristics," *Proc. IRE*, vol. 45, pp. 1228-1243, 1957.
- [10] C. D. Bulucea and D. Prisecaru, "The calculation of the avalanche multiplication factor in silicon p-n junctions taking into account the carrier generation (thermal or optical) in the space-charge region," *IEEE Trans. Electron Devices*, vol. ED-20, no. 8, pp. 692-701, 1973.
- [11] G. A. M. Hurkx, "On the modelling of tunnelling currents in reverse-biased p-n junctions," *Solid-State Electron.*, vol. 32, no. 8, pp. 665-668, 1989.
- [12] P. U. Calzolari and S. Graffi, "A theoretical investigation on the generation current in silicon p-n junctions under reverse bias," *Solid-State Electron.*, vol. 15, pp. 1003-1011, 1972.
- [13] A. G. Chynoweth, "Ionization rates for electrons and holes in silicon," *Phys. Rev.*, vol. 109, pp. 1537-1540, 1958.
- [14] M. Shur, "Recombination current in forward-biased p-n junctions," *IEEE Trans. Electron Devices*, vol. 35, no. 9, pp. 1564-1565, 1988.
- [15] H. C. de Graaff and F. M. Klaassen, *Compact Transistor Modelling for Circuit Design*. Vienna, Austria: Springer, 1990.
- [16] S. M. Sze, *Physics of Semiconductor Devices*. New York: Wiley, 1981.
- [17] R. Hall, "Temperature coefficient of the breakdown voltage of silicon p-n junctions," *Int. J. Electron.*, vol. 22, no. 6, pp. 513-519, 1967.
- [18] W. J. Kloosterman and H. C. de Graaff, "Avalanche multiplication in a compact bipolar transistor model for circuit simulation," *IEEE Trans. Electron Devices*, vol. 36, no. 7, pp. 1376-1380, 1989.

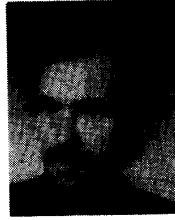
- [19] H. C. Poon and J. C. Meckwood, "Modeling of avalanche effect in integral charge control model," *IEEE Trans. Electron Devices*, vol. ED-19, no. 1, pp. 90-97, 1972.
- [20] W. Groebner and N. Hofreiter, *Integraltafel, zweiter Teil: Bestimmte Integrale*. Vienna, Austria: Springer, 1961, p. 162.

field of interest is device modeling for circuit simulation. Since his retirement from Philips Research (Nov. 1991) he has been a consultant to the University of Twente and the Technical University of Delft, both in The Netherlands.



**G. A. M. Hurkx** was born in Best, The Netherlands, in 1956. He received the M.S. degree in physical engineering in 1985 and the Ph.D. degree in 1991, both from the Eindhoven University of Technology, Eindhoven, The Netherlands.

He joined Philips Research Laboratories, Eindhoven, in 1979 and has been involved in semiconductor research since 1983. His present field of interest is the modeling and simulation of bipolar devices.



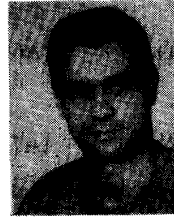
**W. J. Kloosterman** was born in Olst, The Netherlands, in July 1951. He graduated from the Technical College in Zwolle in 1974.

He joined Philips Research Laboratories, Eindhoven, The Netherlands, in 1974. First he worked on finite-element methods in mechanical engineering, and, since 1980, has been involved in CACD, transistor modeling, and parameter extraction.



**H. C. de Graaff** was born in Rotterdam, The Netherlands, in 1933. He received the M.S. degree in electrical engineering from the Delft University of Technology, Delft, The Netherlands, in 1956, and the Ph.D. degree from the Eindhoven University of Technology, Eindhoven, The Netherlands, in 1975.

He joined Philips Research Laboratories, Eindhoven, in 1964, and has been working on thin-film transistors, MOST, bipolar devices, and materials research on polycrystalline silicon. His present



**M. P. G. Knuvers** was born in Drunen, The Netherlands, in February 1962. He graduated from the Technical College of Eindhoven, Eindhoven, The Netherlands in 1987.

He joined Philips Research Laboratories, Eindhoven, in 1987 and is presently involved in the modeling and simulation of bipolar devices.